The Tension Stiffening Mechanism in Reinforced Concrete Prisms

by

Rahimah Muhamad, M.S. Mohamed Ali, Deric John Oehlers and Michael Griffith

*Reprinted from*

**Advances in Structural Engineering**

***Volume 15 No. 12 2012***

MULTI-SCIENCE PUBLISHING CO. LTD.
5 Wates Way, Brentwood, Essex CM15 9TB, United Kingdom

# The Tension Stiffening Mechanism in Reinforced Concrete Prisms

**Rahimah Muhamad, M.S. Mohamed Ali*, Deric John Oehlers and Michael Griffith**

School of Civil, Environmental and Mining Engineering, University of Adelaide, South Australia 5005, Australia

(Received: 19 August 2011; Received revised form: 5 March 2012; Accepted: 29 March 2012)

**Abstract:** Tension stiffening is an important phenomenon in reinforced concrete because it controls not only deflections but also crack spacings, crack widths and the formation of multiple cracks. It is now common practice to study the effects of tension stiffening in concentrically loaded prisms, which is the subject of this paper, and use these behaviours as guidance for the effects of tension stiffening in reinforced concrete beams. As tension stiffening is a mechanism for stress transfer between the concrete and reinforcement, the interface bond stress-slip ($\tau$–$\delta$) properties are of utmost importance. In this paper, partial interaction theory is used to develop generic closed form solutions for crack spacings and widths, the load to cause primary, secondary cracks and subsequent cracks. Four different types of interface bond characteristics ($\tau$–$\delta$) are considered: a *linear ascending* bond slip which is useful at serviceability; a *linear descending* bond slip which is useful at the ultimate limit state; a *nonlinear* bond slip characteristic which closely resembles material bond slip behavior at all limits; and the CEB-FIP Model Code 90 (CEB 1992).

**Key words:** reinforced concrete, tension stiffening, partial interaction, deflections, crack spacings, crack widths, bond stress slip.

## 1. INTRODUCTION

The tension stiffening effect has been widely used in predicting the tensile behaviour of reinforced concrete prisms (Beeby and Scott 2005; Chan *et al*. 1992; Goto 1971; Gupta and Maestrini 1990; Hegemier *et al*. 1985; Jiang *et al*. 1984; Lee and Kim 2008; Marti *et al*. 1998; Mirza and Houde 1979; Rizkalla and Hwang 1984; Somayaji and Shah 1981; Yankelevsky *et al*. 2008). It is not only important in controlling the deflection of beams (Bischoff 2005; Gilbert 2007) but also can be utilised for predicting multiple crack spacings and crack widths (Bischoff *et al*. 2003; Kong *et al*. 2007; Wu *et al*. 2009). The tension stiffening effect allows the stress transfer from the reinforcement to the surrounding concrete through the interface bond stress slip property ($\tau$–$\delta$). Hence, the concrete stress is gradually increasing due to this process and also vice versa for stress in the reinforcement. This stress transfer process continues until the tensile capacity of the concrete is reached after which cracks occur. Therefore, the tension stress carried by the concrete at any section is important in determining the location of cracks.

This tensile concrete stress is directly related to the interface bond stress slip property which shows that the bond stress is significant in modelling (Cosenza *et al*. 1997; Elighausen *et al*. 1983) or deriving a governing equation for predicting these behaviours (Mohamed Ali *et al*. 2008a; Oehlers *et al*. 2005; Oehlers *et al*. 2011b). An interface bond stress $\tau$ distribution along the reinforcement rather than an interface bond slip material property $\tau$–$\delta$ for predicting the crack spacing and crack width has been used (Chan *et al*. 1992; Somayaji and Shah 1981). This was a good starting position in the analysis of tension stiffening. However, as the bond

*Corresponding author. Email address: mmsadakk@civeng.adelaide.edu.au; Fax: +61-8-8303-4359; Tel: +61-8-8303-3968.

stress distribution depends on the bond slip properties $\tau$–$\delta$ which can vary considerably (Seracino *et al*. 2007) as well as the size and type of reinforcement (Mohamed Ali *et al*. 2008a; Oehlers *et al*. 2005; Oehlers *et al*. 2011a) this approach will not provided generic solutions.

A more advanced approach is to use a specific bond slip property $\tau$–$\delta$. The concept of tension stiffening has been used by Marti *et al*. (1998) and Warner *et al*. (2007) and is referred to as the tension chord model. In their model, the following very simplistic assumptions are made to obtain a solution. A stepped-rigid plastic $\tau$–$\delta$ model is proposed to describe the slip between the reinforcement and concrete in which there is a uniform bond stress slip in the unyielded region and a reduced uniform bond stress slip in the yielded region; this change in bond strength suggests that the bond properties are not just a material property. Also they made the assumption that the strain in the concrete between cracks is relatively small and can be ignored which limits the accuracy of the model as the strain in the concrete is no longer related to the formation of cracks. Other researchers have proposed that the bond stress slip is uniform (Choi and Cheung 1996; Gupta and Maestrini 1990; Wu *et al*. 1991) which is probably better than assuming it is dependent on yield as it is now a material property but still an over simplification.

Extensive experimental investigations into simulating the tension stiffening effects of reinforced concrete prisms have been carried out (Bischoff 2003; Jiang *et al*. 1984; Lee and Kim 2008; Mirza and Houde 1979; Rizkala and Hwang 1984; Somayaji and Shah 1981; Tastani and Pantazopoulou 2010; Wu *et al*. 2008; Yankelevsky *et al*. 2008). These tests provide a range of data that has been used to analyse the crack spacings and crack widths in order to develop empirical formulae used in CEB-FIP Model Code 90 (CEB 1992), Eurocode-2 (2004) and by Marti *et al*. (1998) as shown in Table 1.

The next step in this research is to develop generic closed form mechanics solutions for crack spacings, crack widths and the loads to cause multiple cracking that is based on bond-slip $\tau$–$\delta$ material characteristics that simulate those from tests. This is the subject of this paper. The governing equations are first presented. Later, these governing equations are solved using the following four wide ranging types of interface bond stress slip $\tau$–$\delta$ characteristics to provide closed form solutions: (1) A *linear ascending* bond-slip variation which is ideally suited for the early stages of serviceability and which provides nice and simple closed form solutions that clearly illustrate the importance of specific parameters at serviceability; (2) A *non-linear* bond-slip which gives complex solutions but closely simulates the shapes of typical experimentally determined bond slip shapes; (3) A bond-slip model based on the same exponential shape as the well accepted CEB-FIB Model Code 90 (CEB 1992) and by Eligehausen *et al*. (1983) and finally (4) A *linear descending* bond-slip variation that is suitable at the ultimate limit state such as in the formation of hinges (Haskett *et al*. 2009a; Mohamed Ali *et al*. 2008b) and which also gives simple closed form solutions and illustrates the parameters that govern at the ultimate limit state.

The aim of this paper is to develop the fundamental mechanics that govern the tension stiffening behaviour for short term loads as it is realised that the short term deflection of reinforced concrete members is the starting position for long term deflection. Hence the accuracy of the long term deflection depends on the accuracy of the short term deflection. Hence this paper is on short term loading. However it will be shown in this paper how time dependent effects can be included.

## 2. GOVERNING EQUATIONS FOR TENSION STIFFENING

The fundamental governing equation for closed form solutions can be derived from the equilibrium equations for any bonded joint such as a reinforced concrete prism under pure tension as shown in Figure 1(a) in which shear lag is ignored as is the usual practice. The derivation of the governing equation for this stress transfer problem involves four unknown fields which are: the axial stresses $\sigma_r = \sigma_r(x)$ in the reinforcement and $\sigma_c = \sigma_c(x)$ in the concrete; the axial strains $\varepsilon_r = \varepsilon_r(x)$ in the reinforcement and $\varepsilon_c = \varepsilon_c(x)$ in the concrete; the interface shear stress across the bonded length $\tau = \tau(x)$; and the interface slip $\delta = \delta(x)$ which is the difference between the axial displacement $u_r$ of the reinforcement and $u_c$ of the concrete (Mohamed Ali *et al*. 2008a; Muhamad *et al*. 2011a; Wu *et al*. 2002; Yuan *et al*. 2004).

From Figures 1(b) and 1(c), the generic equilibrium equations for a reinforced prism under pure tension can be written as

$$\frac{d\sigma_r}{dx} = \frac{\tau L_p}{A_r} \tag{1a}$$

and

$$\frac{d\sigma_c}{dx} = -\frac{\tau L_p}{A_c} \tag{1b}$$

**Table 1. Published crack spacings and widths**

| Model | Crack spacing | Crack width |
|---|---|---|
| Eurocode2 (2004) | $S_{r,\max} = 3.4C + 0.425k_1k_2\left(\frac{d_b}{\rho_{eff}}\right)$<br>where<br>$S_{r,\max}$ = maximum crack spacing<br>$k_1$ = coefficient of the bond properties of the bars<br>$k_2$ = coefficient of distribution of tensile stress<br>$d_b$ = bar diameter<br>$C$ = concrete cover<br>$\rho_{eff}$ = effective reinforcement ratio | $w_k = S_{r,\max}\left(\varepsilon_{sm} - \varepsilon_{cm}\right)$<br>where<br>$w_k$ = crack width<br>$\varepsilon_{sm} - \varepsilon_{cm}$ = different between mean strain of steel and concrete |
| CEB-FIP Code Model (CEB.1992) | $S_{rm} = \frac{\sigma_{s2}}{2\tau_{bk}} d_b \frac{1}{1+\alpha_e\rho_{sef}}$<br>where<br>$\sigma_{s2}$ = steel stress at the crack<br>$\tau_{bk}$ = lower fractile value of the average bond stress = $1.8f_{ctm}(t)$ (short term loading)<br>$f_{ctm}(t)$ = mean value of the tensile strength of the concrete at the time $t$ when the crack appeared $1+ \alpha_e \rho_{sef} = 1$(for simplicity) | $w_{rm} = S_{rm}\ \varepsilon_{sm}$<br>where<br>$\varepsilon_{sm}$ = average strain of the reinforcement |
| Marti *et al*. 1998 | $S_{rm} = \lambda\frac{\phi f_{ct}}{2\tau_{bo}\rho}$<br>where<br>$S_{rm}$ = crack spacing<br>$\rho$ = reinforcement ratio of tension chord<br>$\tau_{bo}$ = average of bond stress = $2f_{ct}$<br>$\phi$ = diameter of reinforcement bar<br>$f_{ct}$ = tensile strength of the concrete | $w = \frac{S_{rm}(2\sigma_{sr} - \lambda\sigma_{sro})}{2E_s}$<br>where<br>$w$ = crack width<br>$\sigma_{sr}$ = maximum steel stress at the crack<br>$\sigma_{sro}$ = steel stress at crack<br>$E_s$ = elastic modulus of the steel<br>$\lambda$ = coefficient of crack spacing |

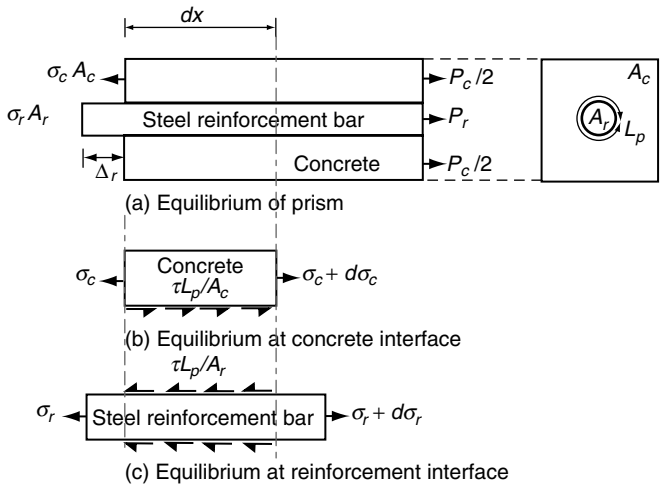


**Figure 1.** Free body diagrams for: (a) equilibrium of prism; (b) equilibrium at concrete interface; and (c) equilibrium at reinforcement interface

and from Figure 1(a), the equation of equilibrium for the prism can be written as

$$\sigma_c A_c + \sigma_r A_r = P_r + P_c \tag{2}$$

where $A_r$ and $A_c$ are the cross-sectional areas of the reinforcement and the concrete respectively and $L_p$ is the circumference of the reinforcement as shown in Figure 1(a). The concrete force $P_c = 0$ as assuming that there is an initial crack. The axial tension force $P_r$ in Eqn 2 will induce a slip at the interface ($\delta$) between the concrete and reinforcement

$$\delta = u_r - u_c \tag{3}$$

Differentiating Eqn 3 gives the following slip strain $\frac{d\delta}{dx}$

$$\frac{d\delta}{dx} = \frac{du_r}{dx} - \frac{du_c}{dx} \tag{4}$$

which for long term loads can be increased by the shrinkage strain. As $\frac{du_r}{dx}$ is simply the reinforcement strain, from the steel and concrete moduli $E_r$ and $E_c$ respectively

$$\sigma_r = E_r \varepsilon_r = E_r \frac{du_r}{dx} \tag{5}$$

and

$$\sigma_c = E_c \varepsilon_c = E_c \frac{du_c}{dx} \tag{6}$$

where $E_r$ and $E_c$ are the elastic modulus of reinforcement and concrete respectively where the latter can be modified to allow for creep under long term loads if required. Substituting Eqns 5 and 6 into 4 yields

$$\frac{d\delta}{dx} = \frac{\sigma_r}{E_r} - \frac{\sigma_c}{E_c} \tag{7}$$

Differentiating Eqn 7, we get

$$\frac{d^2\delta}{dx^2} = \frac{1}{E_r}\left(\frac{d\sigma_r}{dx}\right) - \frac{1}{E_c}\left(\frac{d\sigma_c}{dx}\right) \tag{8}$$

and substituting Eqns 1(a) and 1(b) into Eqn 8 yields the following governing equation

$$\frac{d^2\delta}{dx^2} - \beta_2 \tau = 0 \tag{9a}$$

where

$$\beta_2 = \frac{L_p}{A_r}\left(\frac{1}{E_r} + \frac{A_r}{E_c A_c}\right) \tag{9b}$$

The governing Eqn 9(a) can be solved using the interfacial bond-slip characteristic $\tau = f(\delta)$ along with the boundary conditions for this specific tension stiffening problem that is shown in Figure 2.

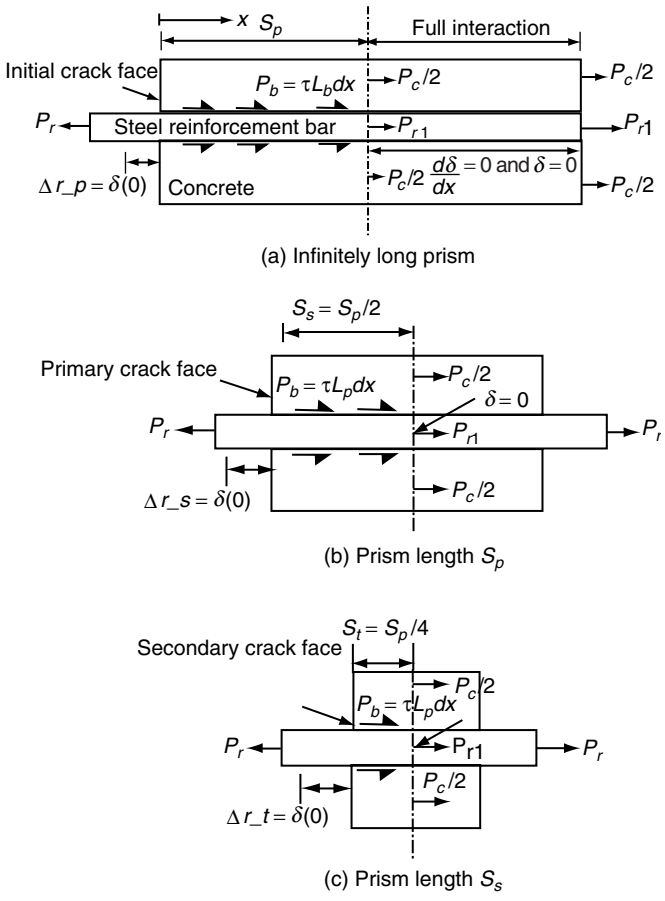


**Figure 2.** Tension stiffening for concrete prism

Figure 2(a) shows the boundary conditions for the formation of primary cracks. Let us assume that there is an initial crack at $x = 0$ beyond which there are no further cracks so it is a question of determining the first series of cracks or primary cracks. At $x = 0$ the strain in the concrete is zero so that the slip strain is simply the strain in the reinforcement, hence

$$\frac{d\delta}{dx} = \frac{P_r}{A_r E_r} \text{ and } \delta = \Delta_r \text{ at } x = 0 \tag{10}$$

$S_p$ in Figure 2(a) is defined as a position beyond which the slip-strain tends to zero that is the start of where the behaviour tends towards full-interaction as shown. Hence

$$\delta = 0 \text{ and } \frac{d\delta}{dx} = 0 \text{ at } x = S_p \tag{11}$$

As full-interaction is first achieved at $x = S_p$, the maximum stress in the concrete is first achieved at $S_p$. Hence the primary crack can occur anywhere in the full-interaction region so that $S_p$ is the minimum crack spacing for the primary cracks. As beams are normally subjected to a moment gradient $S_p$ is also the primary crack spacing.

Primary cracks will occur at a spacing of $S_p$ along the length of the prism. Once these primary cracks have formed, the problem now changes to that shown in Figure 2(b) which is that of a symmetrically loaded prism of length $S_p$. By symmetry, the boundary condition at the mid-length of the prism is given by

$$\delta = 0 \text{ and } \frac{d\delta}{dx} \neq 0 \text{ at } x = S_p/2 = S_s \tag{12}$$

where $S_s$ in Eqn 12 and Figure 2(b) is a secondary crack spacing

Once secondary cracks have formed, the prism length now changes to that shown in Figure 2(c). By symmetry, the cracks occurs at a crack spacing of $S_p/4$ whenever the bond is adequately strong, the boundary condition at this stage can be written as

$$\delta = 0 \text{ and } \frac{d\delta}{dx} \neq 0 \text{ at } x = S_p/4 = S_t \tag{13}$$

where $S_t$ in Eqn 13 and Figure 2(c) is a tertiary crack spacing

Figures 2(a), (b) and (c) also illustrate the random nature of cracking. It has already been explained that the first primary crack can occur anywhere in the full interaction region in Figure 2(a) but will probably occur closer to $S_p$ due to the moment gradient in the beam. Hence cracks can occur in any position beyond $S_p$ from the initial crack and tests on beams would suggest that the crack spacing can be as large as $2S_p$. If, for example, the crack spacing is $2S_p$, then the prism in Figure 2(b) would be $2S_p$ long so by symmetry the next crack would occur at $2S_p/2$ and the next in Figure 2(c) at $2S_p/4$. If, as a further example, the crack spacing is $1.4S_p$, then the next crack would occur at $1.4S_p/2$ and the next at $1.4S_p/4$. In the following analyses, it has been assumed that the initial crack spacing is the minimum crack spacing $S_p$ but this could be adjusted to a factor of $S_p$ and applied using the same boundary condition as in Figure 2(b). It is also worth noting at this stage, that it will be shown that the formation of primary, secondary and tertiary cracks, as in Figures 2(a), (b) and (c), depends on the bond strength. For example the bond may be sufficient to form primary cracks in Figure 2(a) but not sufficient to form secondary cracks as in Figure 2(b) as the bonded length in Figure 2(b) is less than that in Figure 2(a). This further adds to the random nature of cracking.

In this paper, the primary and secondary crack spacings, crack widths as well as the load to cause cracks have been derived for the four different types of interfacial bond stress slip characteristics $\tau$–$\delta$ as shown in Figure 3 and which consist of the following. Firstly a *linear ascending* bond slips property represented by O-B in Figure 3 that has a stiffness $k_e$. Secondly a *non-linear* bond slip property represented by O-B'-E which is characterised by an ascending nonlinear curve with a peak shear stress of $\tau_{max}$ at a slip of $\delta_2$ and a descending non-linear curve. Thirdly the bond slip property of CEB-FIP Model Code 90 (CEB 1992) and Eligehausen *et al.* (1983) for an *ascending non-linear* curve with a peak shear stress of $\tau_{max}$ at a slip of $\delta_1$ represented by O-B. And finally the *linear descending* bond slip property with a peak shear stress of $\tau_{max}$ at a slip of zero and a peak slip of $\delta_{max}$ at a zero shear stress $\tau$ represented by O-A-C in Figure 3.

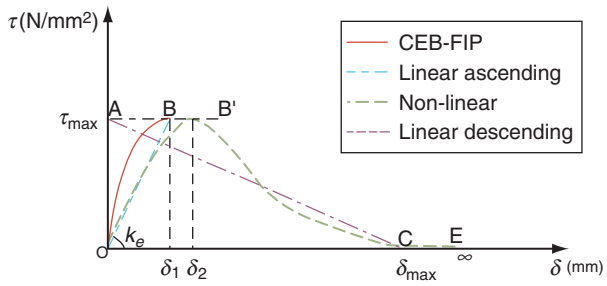


**Figure 3.** Idealised bond stress slip characteristics

## 3. SOLUTIONS FOR LINEAR ASCENDING BOND SLIP CHARACTERISTIC

The bond stress slip for a *linear ascending* characteristic (Mohamed Ali *et al*. 2008a; *Wu et al*. 2002; Yuan *et al*. 2004), as depicted by O-B in Figure 3, can be written as follows

$$\tau = k_e \delta \tag{14}$$

where $k_e$ is the stiffness of the bond slip property $\tau$–$\delta$.

Substituting Eqn 14 into the governing equation of Eqn 9(a) yields

$$\frac{d^2\delta}{dx^2} = \beta_2 k_e \delta \tag{15}$$

Solving the differential equation of Eqn 15 gives the slip variation

$$\delta(x) = c_1 \cosh(\lambda_1 x) + c_2 \sinh(\lambda_1 x) \tag{16a}$$

where

$$\lambda_1 = \sqrt{k_e \beta_2} \tag{16b}$$

Differentiating Eqn 16(a) yields

$$\frac{d\delta}{dx} = \lambda_1 c_1 \sinh(\lambda_1 x) + \lambda_1 c_2 \cosh(\lambda_1 x) \tag{17}$$

Substituting Eqn 16(a) into the *linear ascending* bond stress slip $\tau$–$\delta$ of Eqn 14 results in

$$\tau(x) = k_e \left[ c_1 \cosh(\lambda_1 x) + c_2 \sinh(\lambda_1 x) \right] \tag{18}$$

in which the constants $c_1$ and $c_2$ in Eqns 16(a)-18 can be solved through the substitution of boundary conditions as follows.

### 3.1. Analysis of Infinitely Long Prism [see Figure 2(a)]

#### 3.1.1. Linear ascending crack spacings and load to cause a crack for infinitely long prism

The boundary condition at the initial crack face in Figure 2(a) is given by Eqn 10. Applying this boundary condition into Eqn 17 yields

$$c_2 = \frac{P_r}{A_r E_r \lambda_1} \tag{19}$$

For the boundary condition in Eqn 11 that is $\delta = 0$ and $d\delta/dx = 0$ at $x = S_p$ [refer Figure 2(a)]. Applying these boundary conditions and Eqns 19 into 16(a) and 17 gives

$$c_1 \cosh(\lambda_1 S_p) + \frac{P_r}{A_r E_r \lambda_1} \sinh(\lambda_1 S_p) = 0 \tag{20}$$

$$\lambda_1 c_1 \sinh(\lambda_1 S_p) + \frac{P_r}{A_r E_r} \cosh(\lambda_1 S_p) = 0 \tag{21}$$

Solving both Eqns 20 and 21 gives the primary crack spacing, $S_p$ as

$$S_p = \frac{2}{\lambda_1} \tag{22}$$

where $S_p \lambda_1 = 2$ is based on an assumption that the bond stress is resisted by 97% of the applied load, $P_r$ (Yuan *et al*. 2004).

Further substitution of Eqns 22 into 21 yields

$$c_1 = -\frac{P_r}{A_r E_r \lambda_1 \tanh 2} \tag{23}$$

The relationship between the force in the bar, $P_r$ at the initial crack at $x = 0$ and the forces in reinforcement and concrete, $P_{r1}$ and $P_c$ at the initiation of a primary crack at $x = S_p$ in Figure 2(a), can be written in the following form

$$P_r - \int_{x=0}^{x=S_p} \tau L_p dx = P_{r1} \tag{24}$$

and

$$P_r = P_{r1} + P_c \tag{25}$$

where the definite integral $\int_{x=0}^{x=S_p} \tau L_p dx$ in Eqn 24 yields the bond force between the concrete and the reinforcement over the length $S_p$.

Solving Eqns 24 and 25 lead to the relationship between the bond force and concrete force as shown below

$$\int_{x=0}^{x=S_p} \tau L_p dx = f_{ct} A_c \tag{26}$$

At $x = S_p$ in Figure 2(a), the slip-strain between the concrete and reinforcement bar is zero which means that the strain in the reinforcement, $\varepsilon_{r1}$, and strain in the concrete, $\varepsilon_c$, are equal from which

$$P_{r1} = \frac{\sigma_c}{E_c} A_r E_r \tag{27}$$

Substituting Eqns 26 and 27 into 24 yields the load to cause a primary crack based on full interaction. Once the tensile stress of the concrete in Eqn 27 reach the tensile strength capacity of the concrete which $\sigma_c = f_{ct}$, the crack will occur and load to cause the crack can be rewritten as

$$P_{r\_cr\_fi} = \frac{f_{ct}}{E_c} A_r E_r + f_{ct} A_c \tag{28}$$

The load to cause a primary crack for infinitely long prism based on partial interaction for *linear ascending* bond stress slip can be obtained by solving the relationship between the bond force and concrete force as shown in Eqn 26. Substituting bond stress of Eqns 18 into 26 which the constants $c_1$ and $c_2$ as shown in Eqns 23 and 19 yield the load to cause a primary crack for infinitely long prism

$$P_{r\_cr\_p} = \frac{A_r E_r \lambda_1^2 f_{ct} A_c}{k_e L_p} \tag{29}$$

#### 3.1.2. Linear ascending load slip behaviour for infinitely long prism

The load $P_r$ and slip at the crack face $\Delta_{r\_p}$ for infinitely long prism in Figure 2(a) can be obtained by substituting Eqns 23 and 19 into slip variation of Eqn 16(a), the slip at the initial crack face, $x = 0$

$$\Delta_{r\_p} = \frac{P_r}{A_r E_r \lambda_1} \tag{30}$$

As the crack width, $w_{r\_p}$ is twice the slip, $\Delta_{r\_p}$ hence the crack width for infinitely long prism as

$$w_{r\_p} = \frac{2P_r}{A_r E_r \lambda_1} \tag{31}$$

### *3.2. Analysis of Prism Length $S_p$ [see Figure 2(b)]*

#### 3.2.1. Linear ascending crack spacing and load to cause a crack for prism length $S_p$

The prism length $S_p$ as shown in Figure 2(b) will be analysed in this section. As the bar of the prism is pulled out, a secondary crack will occur. By symmetry in Figure 2(b), the secondary crack spacing $S_s = S_p/2 = 1/\lambda_1$ can be obtained. Substituting Eqns 19 and 12 into 16(a) will leads to the constant $c_{1\_s}$ that corresponds to the prism length $S_p$ as

$$c_{1\_s} = -\frac{P_r}{A_r E_r \lambda_1} \tanh(1) \tag{32}$$

Substituting Eqns 32 and 19 into 18 and further into Eqn 26 for boundary limit $x = 0$ and $x = S_s$ yield the load to cause a secondary crack for prism length $S_p$

$$P_{r\_cr\_s} = \frac{A_r E_r \lambda_1^2 f_{ct} A_c}{0.35 k_e L_p} \tag{33}$$

#### 3.2.2. Linear ascending behaviour of prism length $S_p$

The load $P_r$ and slip at the primary crack face $\Delta_{r\_s}$ for prism length $S_p$ in Figure 2(b) can be obtained by substituting constants $c_2$ and $c_{1\_s}$ as shown in Eqns 19 and 32 respectively into Eqn 16(a) at $x = 0$ to give

$$\Delta_{r\_s} = \frac{P_r \tanh(1)}{A_r E_r \lambda_1} \tag{34}$$

As the crack width $w_{r\_s} = 2\ \Delta_{r\_s}$ hence the crack width for the prism length $S_p$ as

$$w_{r\_s} = \frac{2P_r \tanh(1)}{A_r E_r \lambda_1} \tag{35}$$

### *3.3. Analysis of Prism Length $S_s$ [see Figure 2(c)]*

#### 3.3.1. Linear ascending crack spacing and load to cause a crack for prism length $S_s$

The prism length $S_s$ in Figure 2(c) can be analysed in this section. By symmetry of the prism, a further tertiary crack will occur at the mid-length of the prism that is $S_t = S_p/4 = 1/2\lambda_1$. Applying the boundary conditions of Eqn 13 and the constant $c_2$ of Eqns 19 into 16(a) yields the unknown constant $c_{1\_t}$ that corresponds to the boundary conditions of Eqn 13 as

$$c_{1\_t} = -\frac{P_r}{A_r E_r \lambda_1} \tanh(0.5) \tag{36}$$

Substituting Eqns 36 and 19 into 18 and further into Eqn 26 for boundary limit $x = 0$ and $x = S_t$, will gives the load to cause a tertiary crack for prism length $S_s$ as

$$P_{r\_cr\_t} = \frac{A_r E_r \lambda_1^2 f_{ct} A_c}{0.113 k_e L_p} \tag{37}$$

### 3.3.2. Linear ascending behaviour of prism length $S_s$

The load $P_r$ and slip $\Delta_{r\_t}$ at the secondary crack face for the prism length $S_s$ in Figure 2(c) can be obtained by substituting constant $c_2$ and $c_{1\_t}$ as shown in Eqns 19 and 36 respectively into Eqn 16(a) at $x = 0$ to give

$$\Delta_{r\_t} = \frac{P_r \tanh(0.5)}{A_r E_r \lambda_1} \tag{38}$$

As the crack width $w_{r\_t} = 2\ \Delta_{r\_t}$ hence the crack width for the prism length $S_s$ as

$$w_{r\_t} = \frac{2P_r \tanh(0.5)}{A_r E_r \lambda_1} \tag{39}$$

## 4. SOLUTIONS FOR NON-LINEAR BOND SLIP CHARACTERISTIC

The *non-linear* bond slip characteristic shown as O-B'-E in Figure 3 was proposed by Dai *et al*. (2006) and can be written as

$$\tau = 4\tau_{\max} e^{-k\delta}(1 - e^{-k\delta}) \tag{40a}$$

where

$$k = \frac{0.693}{\delta_2} \tag{40b}$$

Substituting Eqn 40(a) into the governing equation of Eqn 9(a) leads to

$$\frac{d^2\delta}{dx^2} = 4\tau_{\max}\beta_2 e^{-k\delta}(1 - e^{-k\delta}) \tag{41}$$

As

$$\frac{d^2\delta}{dx^2} = \frac{d}{dx}\left(\frac{d\delta}{dx}\right) = \frac{d\nu}{dx} = \frac{d\nu}{d\delta}\left(\frac{d\delta}{dx}\right) = \nu\frac{d\nu}{d\delta} \tag{42a}$$

where

$$\nu = \frac{d\delta}{dx} \tag{42b}$$

using Eqn 42(a) and substituting into Eqn 41 leads to

$$\nu\frac{d\nu}{d\delta} = 4\tau_{\max}\beta_2 e^{-k\delta}(1 - e^{-k\delta}) \tag{43}$$

Rearranging Eqn 43 and integrating both side of the equation yields

$$\frac{d\delta}{dx} = A\sqrt{-2e^{-k\delta} + e^{-2k\delta} + c_3} \tag{44a}$$

where

$$A = 2.4\sqrt{\tau_{\max}\delta_2\beta_2} \tag{44b}$$

and $c_3$ is a constant of integration.

For the boundary conditions of Eqn 11 which $\frac{d\delta}{dx} = 0$ and $\delta = 0$ at $x = S_p$, unknown constant $c_3$ in Eqn 44(a) can be determined. Thus, Eqn 44(a) can be written as

$$\frac{d\delta}{dx} = A(1 - e^{-k\delta}) \tag{45}$$

Rearranging Eqn 45 yields

$$\frac{e^{k\delta}d\delta}{e^{k\delta} - 1} = Adx \tag{46}$$

Integrating both side of Eqn 46 will gives the variation of slip

$$\delta(x) = \frac{1}{k}\ln\left(e^{k(Ax + c_4)} + 1\right) \tag{47}$$

where $c_4$ is a constant of integration.

Differentiating Eqn 47 will lead to the following variation of slip strain as

$$\frac{d\delta(x)}{dx} = A\frac{e^{k(Ax + c_4)}}{e^{k(Ax + c_4)} + 1} \tag{48}$$

and variation of bond stress as

$$\tau(x) = 4\tau_{\max} e^{-k\delta(x)}\left(1 - e^{-k\delta(x)}\right) \tag{49}$$

The unknown $c_4$ in Eqns 47 and 48 can be solved through substitution of boundary conditions as in following section.

### *4.1. Analysis of Infinitely Long Prism [see Figure 2(a)]*

#### 4.1.1. Non-linear primary crack spacing and load to cause a crack

At the initial crack face of the prism, $x = 0$ in Figure 2(a), applying the boundary condition of Eqns 10 into 48 yields

$$c_4 = \frac{\ln\left(\dfrac{P_r}{AA_rE_r - P_r}\right)}{k} \tag{50}$$

At $x = S_p$ in Figure 2(a), applying the boundary condition of Eqn 11 that is the behaviour tends to full interaction ($\delta = 0$ and $d\delta/dx = 0$) and Eqns 50 into 47 and 48 gives the primary cracks spacing as

$$S_p = -\frac{1}{\sqrt{0.693\beta_2 \dfrac{\tau_{\max}}{\delta_2}}} \tag{51}$$

In solving both Eqns 47 and 48 for boundary conditions $\delta = 0$ and $d\delta/dx = 0$, $e^{AkS_p}$ cannot be zero hence an assumption ($e^{AkS_p} = 0.135$) has to be made to obtain the crack spacing.

Substituting Eqns 50 into 47 and further into Eqn 49 yields the bond stress variation. Furthermore, substituting the bond stress variation into the relationship between the bond force and concrete force of Eqn 26 yields the following load to cause a primary crack for infinitely long prism

$$P_{r\_cr\_p} = 0.5c_5 - \frac{0.124c_5c_6}{\tau_{\max}L_p} - \frac{c_6}{6.94\tau_{\max}L_p} \sqrt{\left(\frac{3.47\tau_{\max}L_pc_5}{c_6}\right)^2 - \frac{19.85\tau_{\max}L_pc_5^{\,2}}{c_6} + 0.74c_5^{\,2}} \tag{52a}$$

where

$$c_5 = AA_rE_r \tag{52b}$$

$$c_6 = f_{ct}A_cAk \tag{52c}$$

#### 4.1.2. Non-linear load slip behaviour for infinitely long prism

The load $P_r$ will induce a slip $\Delta_{r\_p}$ at the initial crack face in Figure 2(a). Slip $\Delta_{r\_p}$ can be obtained by substituting Eqns 50 into 47 at $x = 0$ as follows

$$\Delta_{r\_p} = \frac{1}{k}\ln\left(\frac{P_r}{AA_rE_r - P_r} + 1\right) \tag{53}$$

As the crack width $w_{r\_p}$ is twice the slip $\Delta_{r\_p}$ hence the crack width for primary cracks

$$w_{r\_p} = \frac{2}{k}\ln\left(\frac{P_r}{AA_rE_r - P_r} + 1\right) \tag{54}$$

### *4.2. Analysis of Prism Length $S_p$ [see Figure 2(b)]*

#### 4.2.1. Non-linear crack spacing and load to cause a crack for prism length $S_p$

The prism length $S_p$ in Figure 2(b) will be considered in this subsection. As the bar of the prism is further pulled out, secondary cracks will occur. By symmetry, the secondary crack spacing $S_s = S_p/2$ in Figure 2(b) where the slip is zero is given in Eqn 12. As the slip strain $d\delta/dx$ is not zero at $x = S_s$, rearranging Eqn 44(a) yields

$$\frac{d\delta}{\sqrt{-2e^{-k\delta} + e^{-2k\delta} + c_3}} = Adx \tag{55}$$

Integrating both sides of Eqn 55 will gives

$$\delta(x) = \frac{1}{k}\ln\left(\frac{\sqrt{c_3 - 1}\sinh\left(\sqrt{c_3}\left(Akx - c_7\right)\right) + 1}{c_3}\right) \tag{56}$$

Applying the boundary conditions in Eqn 12 to Eqns 56 and 44(a) yields the unknown constant $c_{7\_s}$

$$c_{7\_t} = S_tAk - \frac{1}{\sqrt{c_3}}\sinh^{-1}\sqrt{c_3 - 1} \tag{57}$$

and the slip strain

$$\frac{d\delta}{dx} = A\sqrt{c_3 - 1} \tag{58}$$

Applying the boundary conditions in Eqns 10 that is $\delta = \Delta_r$ at $x = 0$ to Eqn 56 yields

$$\Delta_r = \frac{1}{k}\ln\left(\frac{1}{c_{8\_s}}\right) \tag{59a}$$

where

$$c_{8\_s} = \frac{c_3}{c_3 + \sqrt{c_3 - 1}\sinh\left(-S_s Ak\sqrt{c_3}\right)} \tag{59b}$$

Substituting Eqns 59(a) into 44(a) for the boundary condition of Eqn 10 in which $d\delta/dx = P_r/A_rE_r$ and $\delta = \Delta_r$ at $x = 0$ yields

$$\left(\frac{P_r}{AA_rE_r}\right)^2 = c_3 - 2c_{8\_s} + {c_{8\_s}}^2 \tag{60}$$

As slip strain $d\delta/dx$ of Eqn 58 is the difference in strain between the strain in the reinforcement $\varepsilon_{r1}$ and strain in the concrete $\varepsilon_c$, thus Eqn 58 can be rewritten as

$$P_{r1} = A_rE_rA\sqrt{c_3 - 1} + \frac{f_{ct}}{E_c}A_rE_r \tag{61}$$

Substituting Eqns 61 into 25 at the stage the concrete is reaches the tensile capacity $P_c = f_{ct}A_c$, yields the following load to cause a secondary crack for the prism length $S_p$

$$P_{r\_cr\_s} = A_rE_rA\sqrt{c_3 - 1} + \frac{f_{ct}}{E_c}A_rE_r + f_{ct}A_c \tag{62}$$

Substituting Eqns 62 into 60 gives the value of constant $c_{3\_s}$ that corresponds to the boundary conditions of Eqn 12

$$\begin{aligned} &1 - 2c_{8\_s} + {c_{8\_s}}^2 - 2\sqrt{c_{3\_s} - 1}\\ &\left(\frac{f_{ct}}{E_cA} + \frac{f_{ct}A_c}{A_rE_rA}\right) = \left(\frac{f_{ct}}{E_cA}\right)^2 +\\ &2\left(\frac{{f_{ct}}^2A_c}{A^2A_rE_rE_c}\right) + \left(\frac{f_{ct}A_c}{A_rE_rA}\right)^2 \end{aligned} \tag{63}$$

### 4.2.2. Non-linear behaviour of prism length $S_p$

The relationship of load-slip $P$–$\Delta$ for the prism length $S_p$ in Figure 2(b) can be obtained by rearranging Eqn 59(a) and further substituting the resulting equation into Eqn 60 to give

$$e^{-2k\Delta_r} - 2e^{-k\Delta_r} = \left(\frac{P_r}{AA_rE_r}\right)^2 - c_{3\_s} \tag{64}$$

Thus the crack width for prism length $S_p$ can be obtained by $w_{r\_s} = 2\,\Delta_{r\_s}$.

## *4.3. Analysis of Prism Length $S_s$ [see Figure 2(c)]*

### 4.3.1. Non-linear behaviour with crack spacing $S_s$ and load to cause a crack

Consider the prism of length $S_s$ in Figure 2(c). By symmetry, the tertiary crack spacing is $S_t = S_p/4$ in Figure 2(c) where the slip is zero as given in Eqn 13. The boundary condition of Eqn 13 in which $\delta = 0$ at $x = S_t = S_p/4$ when applied to Eqn 56 will give the unknown constant $c_{7\_t}$ that corresponds to the boundary condition of Eqn 13

$$c_{7\_t} = S_tAk - \frac{1}{\sqrt{c_3}}\sinh^{-1}\sqrt{c_3 - 1} \tag{65}$$

Substituting Eqns 65 into 56 for the boundary condition $\delta(x) = \Delta_r$ at $x = 0$ yields

$$\Delta_r = \frac{1}{k}\ln\left(\frac{1}{c_{8\_t}}\right) \tag{66a}$$

where

$$c_{8\_t} = \frac{c_3}{c_3 + \sqrt{c_3 - 1}\sinh\left(-S_tAk\sqrt{c_3}\right)} \tag{66b}$$

Substituting Eqn 66(a) into Eqn 44(a) for the boundary condition of Eqn 10 in which $d\delta/dx = P_r/A_rE_r$ and $\delta = \Delta_r$ at $x = 0$ yields

$$\left(\frac{P_r}{AA_rE_r}\right)^2 = c_3 - 2c_{8\_t} + {c_{8\_t}}^2 \tag{67}$$

Substituting Eqn 62 into Eqn 67 gives the value of constant $c_{3\_t}$ that corresponds to the boundary conditions of Eqn 13

$$\begin{aligned} &1 - 2c_{8\_t} + {c_{8\_t}}^2 - 2\sqrt{c_{3\_t} - 1}\left(\frac{f_{ct}}{E_cA} + \frac{f_{ct}A_c}{A_rE_rA}\right)\\ &= \left(\frac{f_{ct}}{E_cA}\right)^2 + 2\left(\frac{{f_{ct}}^2A_c}{A^2A_rE_rE_c}\right) + \left(\frac{f_{ct}A_c}{A_rE_rA}\right)^2 \end{aligned} \tag{68}$$

The load to cause a tertiary crack for prism length $S_s$ is given by Eqn 62 with $c_3 = c_{3\_t}$ from Eqn 68.

#### 4.3.2. Non-linear behaviour of prism length $S_s$

The relationship of load-slip $P$–$\Delta$ for the prism length $S_s$ in Figure 2(c) is given in Eqn 64 where $c_{3\_t}$ is corresponding to the boundary conditions of Eqn 13 as shown in Eqn 68. Thus the crack width for prism length $S_s$ can be obtained by $w_{r\_t} = 2\ \Delta_{r\_t}$.

## 5. SOLUTIONS FOR NONLINEAR CEB-FIP BOND SLIP CHARACTERISTIC

The *ascending non-linear* curve of bond stress for the CEB-FIP Code Model 90 (CEB 1992) and Eligehausen *et al*. (1983) shown as O-B in Figure 3 can be written as

$$\tau = \tau_{\max}\left(\frac{\delta}{\delta_1}\right)^{\alpha} \tag{69}$$

Substituting bond stress of Eqn 69 into governing equation of Eqn 9(a) leads to

$$\frac{d^2\delta}{dx^2} = \beta_2\tau_{\max}\left(\frac{\delta}{\delta_1}\right)^{\alpha} \tag{70}$$

Using Eqn 42(a), Eqn 70 can be rewritten as

$$v\frac{dv}{d\delta} = \beta_2\tau_{\max}\left(\frac{\delta}{\delta_1}\right)^{\alpha} \tag{71}$$

Rearranging Eqn 71 and integrating both sides of the equation yields

$$\frac{d\delta}{dx} = \sqrt{\frac{2\lambda_2\delta^{1+\alpha}}{1+\alpha} + 2c_9} \tag{72a}$$

where

$$\lambda_2 = \frac{\beta_2\tau_{\max}}{\delta_1{}^{\alpha}} \tag{72b}$$

and $c_9$ is a constant of integration.

Rearranging Eqn 72(a) and further integrating the equation yields

$$\delta\left(Hyp_2F_1\left[\frac{1}{2},\frac{1}{1+\alpha},1+\frac{1}{1+\alpha},-\frac{\lambda_2\delta^{1+\alpha}}{c_9}\right]\right) = \left(x+c_{10}\right)\sqrt{2c_9} \tag{73a}$$

where $Hyp_2F_1$ represents a $2F_1$ hypergeometric function and it is a series of slip function. Solving that slip series functions in mathlab, an assumption has been made that this series is approximately 1.0 hence the slip variation in Eqn 73(a) can be rewritten as

$$\delta = \left(x+c_{10}\right)\sqrt{2c_9} \tag{73b}$$

### *5.1. Analysis of Infinitely Long Prism [see Figure 2(a)]*

#### 5.1.1. CEB model primary crack spacing and load to cause for infinitely long prism

For the boundary conditions of Eqn 11, in which $\delta = 0$ at $x = S_p$, the constant $c_{10}$ in Eqn 73(b) can be obtained as

$$c_{10} = -S_p \tag{74}$$

Substituting Eqn 74 into the slip variation of Eqn 73(b) and further into the bond force and concrete force relationship of Eqn 26 gives the primary crack spacing

$$S_p = \left[\frac{(1+\alpha)f_{ct}A_c\delta_1{}^{\alpha}}{\tau_{\max}L_p\left(\sqrt{2c_9}\right)^{\alpha}}\right]^{\frac{1}{1+\alpha}} \tag{75}$$

Substituting the boundary conditions of Eqn 10 into the slip strain variation of Eqn 72(a) and slip variation of Eqn 73(b), will lead to the constant $c_{9\_p}$

$$c_{9\_p} - \frac{\sqrt{2c_{9\_p}}f_{ct}A_c\lambda_2\delta_1{}^{\alpha}}{\tau_{\max}L_p} = -0.5\left(\frac{P_r}{A_rE_r}\right)^2 \tag{76}$$

where $P_r$ in Eqn 76 is the load to cause the primary crack spacing $S_p$ that is $P_r = P_{r\_cr}$ Substituting the load to cause a primary crack $P_{r\_cr}$ from Eqns 28 into 76 will give the constant $c_{9\_p}$

$$c_{9\_p} - \frac{\sqrt{2c_{9\_p}}f_{ct}A_c\lambda_2\delta_1{}^{\alpha}}{\tau_{\max}L_p} = -0.5\left(\frac{f_{ct}}{E_c} + \frac{f_{ct}A_c}{A_rE_r}\right)^2 \tag{77}$$

#### 5.1.2. CEB model load slip behavior for infinitely long prism

The load $P_r$ and the slip $\Delta_r$ at the initial crack face in Figure 2(a) can be obtained by applying the boundary

conditions of Eqn 10 in which $d\delta/dx = P_r/A_rE_r$ and $\delta = \Delta_r$ at $x = 0$ into the slip strain of Eqn 72(a)

$$\frac{\lambda_2 \Delta_r{}^{1+\alpha}}{1+\alpha} + 0.5\left(\frac{\Delta_r}{S_p}\right)^2 = 0.5\left(\frac{P_r}{A_rE_r}\right)^2 \tag{78}$$

Thus the crack width for prism length $S_p$ can be obtained by $w_{r\_p} = 2\,\Delta_{r\_p}$.

### 5.2. Analysis of Prism Length $S_p$ [see Figure 2(b)]

#### 5.2.1. CEB-FIP model crack spacing and load to cause a crack for prism length $S_p$

The prism length $S_p$ in Figure 2(b) will be analysed. As the bar of the prism is further pulled out, secondary cracks will occur. By symmetry in Figure 2(b), the secondary crack spacing $S_s = S_p/2$ and applying the boundary condition of Eqns 12 into 73(b) will leads to the constant $c_{10\_s}$ corresponding to the prism length $S_p$

$$c_{10\_s} = -S_s \tag{79}$$

Substituting Eqn 79 into the slip variation of Eqn 73(b) and further into the bond force and concrete force relationship of Eqn 26 gives the constant $c_{9\_s}$ that corresponds to the prism of length $S_p$

$$c_{9\_s} = 0.5\left[\frac{(1+\alpha) f_{ct} A_c \delta_1{}^{\alpha}}{\tau_{\max} L_p \left(S_s\right)^{1+\alpha}}\right]^{\frac{2}{\alpha}} \tag{80}$$

Substituting the constant $c_{9\_s}$ of Eqn 80 and also Eqn 79 into the slip variation of Eqn 73(b) at $x = 0$ yields the following slip at the occurrence of the secondary crack for the prism of length $S_p$

$$\Delta_{r\_cr\_s} = S_s\left(\frac{A_c f_{ct} \delta_1{}^{\alpha}(1+\alpha)}{\tau_{\max} L_p \left(S_s\right)^{1+\alpha}}\right)^{\frac{1}{\alpha}} \tag{81}$$

Applying the boundary conditions of Eqn 10 and also Eqn 81 into Eqn 72(a) yields the following load to cause a secondary crack for the prism length $S_p$

$$P_{r\_cr\_s} = A_r E_r \sqrt{\frac{2\lambda_2}{1+\alpha}\left(S_s\right)^{1+\alpha}\left(\frac{(1+\alpha) f_{ct} A_c \delta_1{}^{\alpha}}{\tau_{\max} L_p \left(S_s\right)^{1+\alpha}}\right)^{\frac{1+\alpha}{\alpha}} + \left(\frac{(1+\alpha) f_{ct} A_c \delta_1{}^{\alpha}}{\tau_{\max} L_p \left(S_s\right)^{1+\alpha}}\right)^{\frac{2}{\alpha}}} \tag{82}$$

#### 5.2.2. CEB model load slip behavior of prism length $S_p$

The load $P_r$ and the slip $\Delta_{r\_s}$ at the primary crack faces in Figure 2(b) can be obtained by substituting the boundary conditions of Eqn 10 in which $d\delta/dx = P_r/A_rE_r$ and $\delta = \Delta_r$ at $x = 0$ into the slip strain of Eqn 72(a). This gives the load-slip relationship as well as crack width as shown in Eqn 78 with replace $S_p = S_s$.

### 5.3. Analysis of Prism Length $S_s$ [see Figure 2(c)]

#### 5.3.1. CEB model crack spacing and load to cause a crack for prism length $S_s$

The prism length $S_s$ in Figure 2(c) will be used in this subsection. By symmetry of the prism, the crack will occur at the mid-length of the prism that is $S_t = S_p/4$. These boundary conditions of Eqn 13 in which $\delta = 0$ at $x = S_p/4$ can be applied and give the load to cause a tertiary crack for prism length $S_s$ as shown in Eqn 82 with replace $S_s = S_t$.

#### 5.3.2. CEB model load slip behaviour of prism length $S_s$

The load $P_r$ and the slip $\Delta_{r\_t}$ at the secondary crack face as well as crack widths in Figure 2(c) can be obtained as shown in Eqn 78 with replace $S_p = S_t$.

## 6. SOLUTIONS FOR LINEAR DESCENDING BOND SLIP CHARACTERISTIC

The bond stress for a *linear descending* bond stress slip characteristic (Haskett *et al*. 2009b) O-A-C in Figure 3 can be written as

$$\tau = \frac{\tau_{\max}}{\delta_{\max}}\left(\delta_{\max} - \delta\right) \tag{83}$$

Substituting Eqn 83 into the governing equation of Eqn 9(a) leads to

$$\frac{d^2\delta}{dx^2} = \lambda_3{}^2(\delta_{\max} - \delta) \tag{84a}$$

where

$$\lambda_3 = \sqrt{\frac{\tau_{\max}}{\delta_{\max}}\beta_2} \tag{84b}$$

Solving the differential equation of Eqn 84(a) gives the slip variation

$$\delta(x) = c_{11}\sin\left(\lambda_3 x\right) + c_{12}\cos\left(\lambda_3 x\right) + \delta_{\max} \tag{85}$$

Differentiating Eqn 85 yields the slip strain variation

$$\frac{d\delta(x)}{dx} = \lambda_3 c_{11}\cos(\lambda_3 x) - \lambda_3 c_{12}\sin(\lambda_3 x) \quad (86)$$

Further substituting Eqn 85 into the bond stress slip $\tau$–$\delta$ of the *linear descending* bond-slip in Eqn 83 result in the bond stress variation

$$\tau(x) = -\frac{\tau_{\max}}{\delta_{\max}}\left[c_{11}\sin(\lambda_3 x) + c_{12}\cos(\lambda_3 x)\right] \quad (87)$$

where the constants $c_{11}$ and $c_{12}$ in Eqns 85 to 87 can be solved through substitution of the boundary conditions as follows.

## 6.1. Analysis of Infinitely Long Prism [see Figure 2(a)]

### 6.1.1. Linear descending crack spacing and load to cause a crack for infinitely long prism

The boundary condition at $x = S_p$ in Figure 2(a) is given in Eqn 11. Substituting these boundary condition into Eqns 85 and 86 yields

$$c_{11} = -\delta_{\max}\sin(\lambda_3 S_p) \quad (88)$$

and

$$c_{12} = -\delta_{\max}\cos(\lambda_3 S_p) \quad (89)$$

Substituting both Eqns 88 and 89 into Eqn 86 and further substituting into Eqn 10 will lead to

$$S_p = \frac{\arcsin\left(\dfrac{P_r}{A_r E_r \lambda_3 \delta_{\max}}\right)}{\lambda_3} \quad (90)$$

where $P_r$ in Eqn 90 is the load to cause the primary crack spacing $S_p$ that is $P_r = P_{r\_cr}$. Substituting both constants of Eqns 88 and 89 into the relationship of the bond force and concrete force as given in Eqn 26 results the load to cause a primary crack

$$P_{r\_cr\_p} = \frac{A_r E_r \lambda_3^{\,2} \delta_{\max} f_{ct} A_c}{\tau_{\max} L_p} \quad (91)$$

Substituting Eqns 91 into 90 gives the primary crack spacing

$$S_p = \frac{\arcsin\left(\dfrac{\lambda_3 f_{ct} A_c}{\tau_{\max} L_p}\right)}{\lambda_3} \quad (92)$$

### 6.1.2. Linear descending load slip behavior for infinitely long prism

The load $P_r$ and slip $\Delta_{r\_p}$ can be obtained by substituting the constants $c_{11}$ and $c_{12}$ in Eqns 88 and 89 into 85 at $x = 0$ as follows

$$\Delta_{r\_p} = -\delta_{\max}\cos\left(\arcsin\left(\frac{P_r}{A_r E_r \lambda_3 \delta_{\max}}\right)\right) + \delta_{\max} \quad (93)$$

Substituting Eqn 93 into $w_r = 2\,\Delta_r$ yields the crack width for infinitely long prism as

$$w_{r\_p} = 2\left(-\delta_{\max}\cos\left(\arcsin\left(\frac{P_r}{A_r E_r \lambda_3 \delta_{\max}}\right)\right) + \delta_{\max}\right) \quad (94)$$

## 6.2. Analysis of Prism Length $S_p$ [see Figure 2(b)]

### 6.2.1. Linear descending crack spacing and load to cause a crack for prism length $S_p$

As the bar of the prism length $S_p$ in Figure 2(b) is pulled out, secondary cracks will occurs. By symmetry, the secondary crack spacing $S_s = S_p/2$. Substituting the boundary conditions of Eqns 10 and 12 into Eqns 86 and 85 respectively gives the constants $c_{11\_s}$ and $c_{12\_s}$ that corresponds to a prism of length $S_p$

$$c_{11\_s} = \frac{P_r}{A_r E_r \lambda_3} \quad (95)$$

and

$$c_{12\_s} = \frac{-\delta_{\max} A_r E_r \lambda_3 - P_r \sin(\lambda_3 S_s)}{\cos(\lambda_3 S_s) A_r E_r \lambda_3} \quad (96)$$

Substituting both constants of Eqns 95 and 96 into 87 and further substituting into Eqn 26 gives the load to cause a secondary crack

$$P_{r\_cr\_s} = \frac{f_{ct} A_c \delta_{\max} \lambda_3^{\,2} A_r E_r \cos(\lambda_3 S_s) - A_r E_r \lambda_3 \tau_{\max} \delta_{\max} L_p \sin(\lambda_3 S_s)}{\tau_{\max} L_p (1 - \cos(\lambda_3 S_s))} \quad (97)$$

### 6.2.2. Linear descending load slip behavior of prism length $S_p$

The load $P_r$ and slip $\Delta_{r\_s}$ relationship for a prism length $S_p$ can be obtained by substituting Eqns 95 and 96 into 85 at $x = 0$

$$\Delta_{r\_s} = \delta_{\max}\left(1 - \frac{1}{\cos(\lambda_3 S_s)}\right) - \frac{P_r}{A_r E_r \lambda_3}\tan(\lambda_3 S_s) \quad (98)$$

As the crack width $w_{r\_s}$ is twice the slip $\Delta_{r\_s}$ hence the crack width for a prism length $S_p$ as

$$w_{r\_s} = 2\left[\delta_{\max}\left(1 - \frac{1}{\cos(\lambda_3 S_s)}\right) - \frac{P_r}{A_r E_r \lambda_3}\tan(\lambda_3 S_s)\right] \quad (99)$$

### 6.3. Analysis of Prism Length $S_s$ [see Figure 2(c)]

#### 6.3.1. Linear descending crack spacing and load to cause a crack for prism length $S_s$

By symmetry of the prism of length $S_s$, the tertiary crack will occur at the mid-length of the prism that is $S_t = S_p/4$. Substituting the boundary condition of Eqns 13 into 85 gives the constant $c_{12\_t}$ that corresponds to a prism length $S_s$ as shown in Eqn 96 with replace $S_s = S_t$.

Substituting Eqn 95 and the constant $c_{12\_t}$ into bond stress variation of Eqn 87 and further into Eqn 26 for the boundary limit from $x = 0$ to $x = S_t$ yields the load to cause a tertiary crack for the prism length $S_s$ as shown in Eqn 97 with replace $S_s = S_t$.

#### 6.3.2. Linear descending load slip behavior of prism length $S_s$

The load $P_r$ and slip $\Delta_{r\_t}$ relationship for the prism of length $S_s$ can be obtained by substituting Eqn 95 and the constant $c_{12\_t}$ into the slip variation of Eqn 85 at $x = 0$ as shown in Eqn 98 with replace $S_s = S_t$. As the crack width $w_r$ is twice the slip $\Delta_r$ hence the crack width for the prism length $S_s$ is given in Eqn 99 with replace $S_s = S_t$.

## 7. SUMMARY AND COMPARISONS

The results of this mechanics based analysis of tension-stiffening have been used to derive the short term deflection of steel reinforced beams (Muhamad *et al.* 2011b), FRP reinforced beams (Oehlers *et al.* 2011b) and the behaviour of hinges (Visintin *et al.* 2012) and give good correlation with test results. However, it is felt that a strength of this mechanics based approach is to isolate the parameters that affect tension-stiffening and this will be studied in this section.

### 7.1. Parametric Comparison

Table 1 lists published crack spacings $S_{rm}$ which, in general, have been derived empirically. It can be seen that the main empirically derived parameters that control crack spacing are: bond properties such as $k_1$; bar diameter $d_b$; ratio of reinforcement area to that of concrete $\rho$; steel stress at crack $\sigma_{s2}$; and the tensile strength of concrete $f_{ct}$. These empirically identified parameters are also those identified in the mechanics models that have been developed in this paper. Take for example the analysis based on the linear ascending bond characteristic in Figure 3 where crack spacing is given by Eqn 22 which can be written as follows

$$S_p = \frac{2}{\sqrt{k_e \frac{L_p}{A_r}\left(\frac{1}{E_r} + \frac{A_r}{E_c A_c}\right)}} \qquad (100)$$

Comparing the parameters in the mechanics model of Eqn 100 with the empirical parameters listed above: $k_e$ in the mechanics model is the bond stiffness and equivalent to the bond property $k_1$ in the empirical model, $L_p$ is the bar circumference used in the mechanics model as opposed to the bar diameter $d_b$ in the empirical model, and $A_r/A_c$ is the reinforcement ratio $\rho$ in the empirical model. The crack spacing of Eqn 100 is the crack spacing of primary cracks which is simply twice the spacing after secondary cracks occur. As the reinforcement bar load to cause primary cracks is given by Eqn 29 and that to cause secondary cracks by Eqn 33, it can be seen that the crack spacing is also dependent on the stress in the bar at the crack that is the parameter $\sigma_{s2}$ in the empirical model. The crack spacing of Eqn 100 for the *linear ascending* bond slip properties as well as that for the *non-linear* bond slip properties of Eqn 51 is not dependent on the tensile strength of the concrete $f_{ct}$. In contrast, that for the CEB-FIP Model Code 90 (CEB 1992), Eqn 75, and that for the *linear descending* bond properties, Eqn 92, is dependent on $f_{ct}$ which explains why some of the empirical models in Table 1 show a dependence on $f_{ct}$ (Marti *et al.* 1998) and others (Eurocode 2 2004; CEB-FIP Model Code 90 1992) do not.

There is a remarkably good agreement on the parameters that control the crack width in the empirical rules in Table 1 where it can be seen that in all three empirical rules the crack width depends on the crack spacing $S_{rm}$ and the reinforcement strain $\varepsilon_{sm}$. The crack width for the *linear ascending* bond-slip properties is given by Eqn 31 which can be written as

$$w_r = \frac{S_p P_r}{A_r E_r} \qquad (101)$$

This mechanics model also depends on the crack spacing $S_p$ and reinforcement strain $P_r/A_rE_r$ and is virtually the same equation as that in Eurocode 2 (2004) in Table 1.

### 7.2. Analysis of Concentrically Loaded Prism

The mechanics based solutions are now used to analyse a concentrically loaded prism, such as that shown in Figure 1, with the steel reinforcement properties of $A_r = 1385$ mm$^2$, $E_r = 200$ GPa and $L_p = 132$ mm, concrete prism properties of $A_c = 2215$ mm$^2$, $E_c = 25$ GPa $f_c = 30$ MPa and $f_{ct} = 2.74$ MPa, and bond-slip properties of $\tau_{max} = 6.85$ MPa, $\delta_1 = 1.5$ mm and $\delta_2 = 2.59$ mm as shown in Figure 4. The CEB-FIP Model Code 90 (CEB.1992) bond-slip property O-B in Figure 4 is Eqn 69

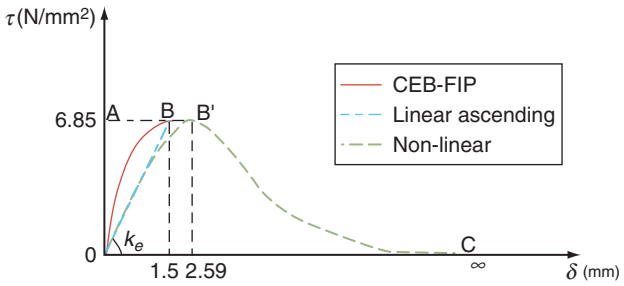


**Figure 4.** Different value of bond stress material properties

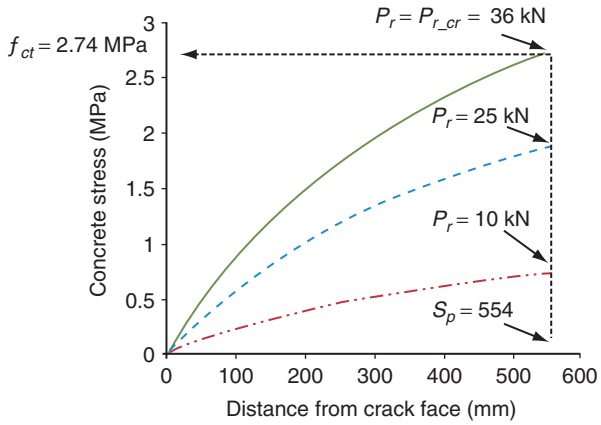


**Figure 5.** Tensile concrete stress along prism length for linear ascending $\tau$–$\delta$

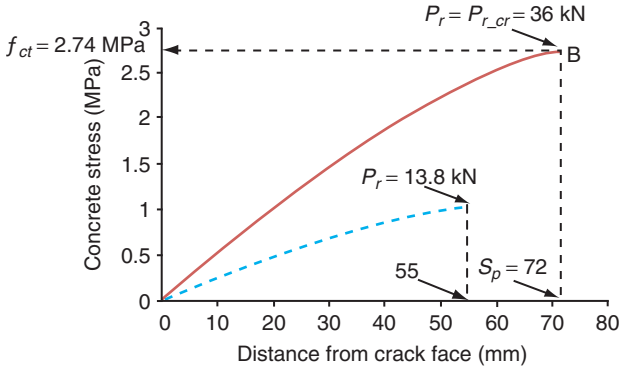


**Figure 6.** Tensile concrete stress along prism for CEB-FIP $\tau$–$\delta$

with the code recommended value for the exponent $\alpha$ in Eqn 69 of 0.4. As the exponent $\alpha$ increases from 0.4 to unity, the CEB-FIB Model Code 90 (CEB 1992) variation approaches that of the *linear ascending* Eqn 14 with the stiffness $k_e$ as shown in Figure 4. The bond stiffness $k_e$ used in Figure 4 is therefore a lower bound to the CEB-FIB Model Code 90 (CEB 1992) stiffness's.

The results of the analysis depicted in Figure 2(a) to determine the crack spacing $S_p$ is shown in Figure 5 for the *linear ascending* bond characteristics in Figure 4. It can be seen in Figure 5 that the concrete stress builds up along the length of the bar and peaks at a distance of 554 mm from the crack face. It can also be seen that the shape of this distribution remains unchanged, that is, it peaks at $S_p = 554$ mm which is independent of the applied load $P_r$. Hence the crack spacing is independent of $f_{ct}$ as Eqn 100 suggests. In contrast for the CEB-FIB Model Code 90 (CEB 1992) bond in Figure 6, the distance from the crack face at which the stress in the concrete peaks is a function of the reinforcement force so that the crack spacing is now a function of the tensile strength of the concrete. Hence it can be seen that the shape of the bond-slip property determines the dependence of the crack spacing on the tensile strength of the concrete which explains why some empirical models in Table 1 include the dependence on $f_{ct}$ and others do not.

The results of analysing a concentrically loaded prism using both the mechanics models developed in this paper and the empirical models in Table 1 are listed in Table 2. The *linear ascending* results are given in

**Table 2. Results from structures mechanics models**

| Bond model | Primary crack spacing* (mm) | Primary crack load (kN) | Secondary crack load (kN) |
|---|---|---|---|
| (1) Linear ascending | 554 | 36 | 103 |
| (2) Non-linear | 438 | 42 | 104 |
| (3) CEB-FIP ($\alpha = 0.4$) | 72 | [36]** | 447 |
| (4) CEB-FIP ($\alpha = 0.5$) | 106 | [36]** | 323 |
| (5) CEB-FIP ($\alpha = 0.6$) | 151 | [36]** | 246 |
| (6) CEB-FIP ($\alpha = 0.99$) | 596 | [36]** | 90 |
| (7) Full interaction | — | [36]** | — |
| (8) Eurocode 2 (2004) | 54 | — | — |
| (9) CEB-FIP Model Code 90 (CEB.1992) | 93 | — | — |
| (10) Marti *et al.* 1998 | 27 | — | — |

* If secondary cracks occur, they will have half this crack spacing

** [ ] values from full interaction value

Row 1. The primary crack spacing is 554 mm and the load to cause this crack is 36 kN which is virtually the same load as that from the *full interaction* analysis Eqn 28 given in Row 7. The reinforcement load has to increase substantially from 36 kN to 103 kN to form secondary cracks. The *non-linear* results in Row 2 are similar to the *linear ascending* results in Row 1. The CEB-FIP Model Code 90 (CEB 1992) bond-slip model recommends at value of $\alpha = 0.4$ as plotted in Figure 4. The results are given in Row 3 where the primary crack spacing is 72 mm, the primary crack load is 36 kN (as this analysis uses the full-interaction results in Eqn 28 and the secondary crack load is 447 kN. The value of $\alpha$ is gradually increased in Rows 4 and 5 where it can be seen that this reduction in bond stiffness causes an increase in the primary crack spacing but a reduction in the secondary crack load. When $\alpha \rightarrow 1$ in Row 6, the bond-slip properties tend to that of the *linear ascending* in Figure 4 so the results in Row 6 in Table 2 tend to the *linear ascending* results in Row 1. The empirical crack spacing in Rows 8 and 9 are similar to that in Row 3 which uses the recommended CEB-FIB Model Code 90 (CEB.1992) bond model. These results emphasise the importance of the bond properties on crack spacing and widths.

## 8. CONCLUSIONS

Generic mechanics based models have been developed for various idealised bond characteristics to predict crack spacings, crack widths and the load to cause primary cracks, secondary cracks and subsequent cracks for short term loads. A comparison between the controlling parameters from the mechanics models and those from empirical models shows that the empirical research has identified the major parameters that affect tension stiffening but that the mechanics equations are too complex to be derived empirically. It is suggested that this research provides an in-depth understanding of tension stiffening and the random nature of cracking and provides the fundamental mechanics parameters that could be calibrated experimentally to develop more accurate design rules. The research also shows how the formation and behavior of primary cracks and subsequent cracks are different due to different boundary conditions.

## ACKNOWLEDGEMENTS

This research was supported by the Australian Research Council Discovery grant DP0985828 “A unified reinforced concrete model for flexure and shear”. The first author also thanks the Universiti Teknologi Malaysia and the Ministry of Higher Education of Malaysia for financial support.

## REFERENCES

Beeby, A.W. and Scott, R.H. (2005). “Cracking and deformation of axially reinforced members subjected to pure tension”, *Magazine of Concrete Research,* Vol. 57, No. 10, pp. 611–621.

Bischoff, P. (2003). “Tension stiffening and cracking of steel fiber-reinforced concrete”, *Journal of Materials in Civil Engineering*, ASCE, Vol. 15, No. 2, pp. 174–182.

Bischoff, P. (2005). “Reevaluation of deflection prediction for concrete beams reinforced with steel and fiber reinforced polymer bars”, *Journal of Structural Engineering,* ASCE, Vol. 131, No. 5, pp. 752–767.

CEB (1992). *CEB-FIP Model Code 9*0, Thomas Telford, London, UK.

Eligehausen, R., Popov, E.P. and Bertero, V.V. (1983). *Local Bond Stress-Slip Relationship of Deformed Bars Under Generalized Excitations*, Report no. UCB/EERC-83/23, Earthquake Engineering Research Center, University of California, Berkeley, CA, USA.

Eurocode-2 (2004). *Eurocode 2: Design of Concrete Structures-Part 1: General Rules and Rules for Buildings*, European Committee for Standardization, Brussels, Belgium.

Chan, H.C., Cheung, Y.K. and Huang, Y.P. (1992). “Crack analysis of reinforced concrete tension members”, *Journal of Structural Engineering*, ASCE, Vol. 118, No. 8, pp. 2118–2132.

Choi, C.K. and Cheung, S.H. (1996). “Tension stiffening model for planar reinforced concrete members”, *Computers & Structures*, Vol. 59, No. 1, pp. 179–190.

Cosenza, E., Manfredi, G. and Realfonzo, R. (1997). “Behaviour and modeling of bond of FRP rebars to concrete”, *Journal of Composites for Construction*, ASCE, Vol. 1, No. 2, pp. 40–51.

Dai, J., Ueda, T. and Sato, Y. (2006). “Unified analytical approaches for determining shear bond characteristics of FRP-concrete interfaces through pull out test”, *Journal of Advanced Concrete Technology*, Vol. 4, No. 1, pp. 133–145.

Gilbert, R.I. (2007). “Tension stiffening in lightly reinforced concrete slabs”, *Journal of Structural Engineering*, ASCE, Vol. 133, No. 6, pp. 899–903.

Goto, Y. (1971). “Cracks formed in concrete around deformed tension bars”, *ACI Journal Proceedings*, Vol. 68, No. 4, pp. 244–251.

Gupta, A.K. and Maestrini, S.R. (1990). “Tension stiffening model for reinforced concrete bars”, *Journal of Structural Engineering*, ASCE, Vol. 116, No. 3, pp. 769–790.

Haskett, M., Oehlers, D.J., Mohamed Ali, M.S. and Wu, C. (2009a). “Rigid body moment-rotation mechanism for reinforced concrete beam hinges”, *Engineering Structures*, Vol. 31, No. 5, pp. 1032–1041.

Haskett, M., Oehlers, D.J., Mohamed Ali, M.S. and Wu, C. (2009b). “Yield penetration hinge rotation in reinforced concrete beams”, *Journal of Structural Engineering*, ASCE, Vol. 135, No. 2, pp. 130–138.

Hegemier, G.A., Murakami, H. and Hageman, L.J. (1985). “On tension stiffening in reinforced concrete”, *Mechanical Materials*, Vol. 4, pp. 161–179.

Jiang, D.H., Shah, S.P. and Andonian, A.T. (1984). "Study of the transfer of tensile forces by bond", *ACI Journal Proceedings*, Vol. 81, No. 3, pp. 251–259.

Kong, K.L., Beeby, A.W., Forth, J.P. and Scott, R.H. (2007). "Cracking and tension zone behaviour in reinforced concrete flexural members", *Proceedings of ICE: Structures and Buildings*, Vol. 160, No. 3, pp. 165–172.

Lee, G.Y. and Kim, W. (2008). "Cracking and tension stiffening behaviour of high strength concrete tension members subjected to axial load", *Advances in Structural Engineering*, Vol. 11, No. 5, pp. 127–137.

Marti, P., Alvarez, M., Kaufmann, W. and Sigrist, V. (1998). "Tension chord model for structural concrete", *Structural Engineering International,* Vol. 8, No. 4, pp. 287–298.

Mirza, S.M. and Houde, J. (1979). "Study of bond stress-slip relationships in reinforced concrete", *ACI Journal Proceedings*, Vol. 76, No. 1, pp. 19–46.

Mohamed Ali, M.S., Oehlers, D.J., Griffith, M.C. and Seracino, R. (2008a). "Interfacial stress transfer of near surface-mounted FRP-to-concrete joints", *Engineering Structures*, Vol. 30, No. 7, pp. 1861–1868.

Mohamed Ali, M.S., Oehlers, D.J. and Griffith, M.C. (2008b). "Simulation of plastic hinges in FRP plated RC beams", *Journal of Composites for Construction*, ASCE, Vol. 12, No. 6, pp. 617–625.

Muhamad, R., Mohamed Ali, M.S., Oehlers, D.J. and Sheikh, A.H. (2011a). "Load-slip relationship of tension reinforcement in reinforced concrete members", *Engineering Structures*, Vol. 33, No. 4, pp. 1098–1106.

Muhamad, R., Oehlers, D.J. and Mohamed Ali, M.S. (2011b) "Discrete rotation deflection of RC beams at serviceability", *Proceedings of ICE: Structures and Buildings*. (in press)

Oehlers, D.J., Liu, I.S.T. and Seracino, R. (2005). "The gradual formation of hinges throughout reinforced concrete beams", *Mechanics Based Design of Structures and Machines*, Vol. 33, No. 3–4, pp. 373–398.

Oehlers, D.J., Mohamed Ali, M.S., Haskett, M., Lucas, W., Muhamad, R. and Visintin, P. (2011a). "FRP reinforced concrete beams – a unified approach based on IC theory", *Journal of Composites for Construction*, ASCE, Vol. 15, No. 3, pp. 293–303.

Oehlers, D.J., Muhamad, R. and Mohamed Ali, M.S. (2011b). "Serviceability flexural ductility of FRP and steel RC beams: a discrete rotation approach", *Construction and Building Materials*. (submitted)

Rizkalla, S.H. and Hwang, L.S. (1984). "Crack prediction for members in uniaxial tension", *ACI Journal Proceedings*, Vol. 81, No. 6, pp. 572–579.

Somayaji, S. and Shah, S.P. (1981). "Bond stress versus slip relationship and cracking response of tension members", *ACI Journal Proceedings*, Vol. 78, No. 3, pp. 217–225.

Seracino, R., Raizal Saifulnaz, M.R. and Oehlers, D.J. (2007). "Generic debonding resistance of EB and NSM plate-to-concrete joints", *Journal of Composites for Construction*, ASCE, Vol. 11, No. 1, pp. 62–70.

Tastani, S.P. and Pantazopoulou, S.J. (2010). "Direct tension pullout bond test: experimental test", *Journal of Structural Engineering*, ASCE, Vol. 136, No. 6, pp. 731–743.

Visintin, P., Oehlers, D.J., Wu, C. and Haskett, M. (2012). "A mechanics solution for hinges in RC beams with multiple cracks", *Engineering Structures*, Vol. 36, No. 3, pp. 61–69.

Warner, R.F., Foster, S.J. and Kilpatrick, A.E. (2007). *Reinforced Concrete Basics: Analysis and Design of Reinforced Concrete Structures*, Pearson Education, Australia.

Wu, H.Q. and Gilbert, R.I. (2008). *An Experimental Study of Tension Stiffening in Reinforced Concrete Members under Short Term and Long Term Loads,* Report No. R-449, University of New South Wales, Sydney, Australia.

Wu, H.Q. and Gilbert, R.I. (2009). "Modelling short-term tension stiffening in reinforced concrete prisms using a continuum-based finite element model", *Engineering Structures*, Vol. 31, No. 10, pp. 2380–2391.

Wu, Z., Yoshikawa, H. and Tanabe, T. (1991). "Tension stiffness model for cracked reinforced concrete", *Journal of Structural Engineering*, ASCE, Vol. 117. No. 3, pp. 715–732.

Wu, Z., Yuan, H. and Niu, H. (2002). "Stress transfer and fracture in different kinds of adhesive joints", *Journal of Engineering Mechanics*, ASCE, Vol. 128, No. 5, pp. 562–573.

Yankelevsky, D.Z., Jabareen, M. and Abutbul, A.D. (2008). "One-dimensional analysis of tension stiffening in reinforced concrete with discrete cracks", *Engineering Struct*ures, Vol. 30, No. 1, pp. 206–217.

Yuan, H., Teng, J.G., Seracino, R. and Wu, Z.S. (2004). "Full range behaviour of FRP-to-concrete bonded joints", *Engineering Structures*, Vol. 26, No. 5, pp. 543–691.